

Measuring Omega*

Avishai Dekel¹, David Burstein², Simon D.M. White³

¹The Hebrew University of Jerusalem

²Arizona State University, Tempe

³Max-Planck-Institut fuer Astrophysik, Garching

1 Introduction

We were asked to debate the value of Ω , the fundamental energy density parameter of cosmology, and in particular its mass component, Ω_m . Is the universe flat and marginally bound with $\Omega_m = 1$ in accordance with the simplest cosmological model? Is Ω_m clearly smaller than unity as seems to be indicated by several observations? Unfortunately, we cannot provide a clear answer at this point because there is conflicting evidence. Entertaining the audience with our biased views on the subject might not be very constructive. Instead, it may be more interesting to lay out the various *methods* used to measure Ω_m , mention new developments and current estimates, and focus on the promising prospects versus the associated difficulties. In the critical discussion that follows we try to shed light on the nature of the uncertainties that may be responsible for the current span of estimates for Ω_m .

We divide the methods into the following four classes:

- *Global measures.* Based on properties of space-time that constrain combinations of Ω_m and the other cosmological parameters (Λ , H_0 , t_0).
- *Virialized Systems.* Methods based on nonlinear dynamics within galaxies and clusters on comoving scales $1 - 10 h^{-1}\text{Mpc}$.
- *Large-scale structure.* Measurements based on mildly-nonlinear gravitational dynamics of fluctuations on scales $10 - 100 h^{-1}\text{Mpc}$ of superclusters and voids, in particular *cosmic flows*.
- *Growth rate of fluctuations.* Comparisons of present day structure with fluctuations at the last scattering of the cosmic microwave background (CMB) or with high redshift objects of the young universe.

The methods and current estimates are discussed below and summarized in Figure 1 and Table 1. The estimates based on virialized objects typically yield low values of $\Omega_m \sim 0.2-0.3$. The global measures, large-scale structure and cosmic flows typically indicate higher values of $\Omega_m \sim 0.4 - 1$.

*To appear in Critical Dialogues in Cosmology (Princeton 250th Anniversary), ed. N. Turok (World Scientific)

2 Global Measures

We adopt as our basic working hypothesis the standard cosmological model of Friedmann Robertson Walker (FRW), where we assume homogeneity and isotropy and describe gravity by general relativity. We limit the discussion to the matter-dominated era in the “dust” approximation.

The Friedmann equation that governs the universal expansion can be written in terms of the different contributions to the energy density (*e.g.*, [1]):

$$\Omega_m + \Omega_\Lambda + \Omega_k = 1 ,$$
$$\Omega_m \equiv \frac{\rho_m}{(3H^2/8\pi G)}, \quad \Omega_\Lambda \equiv \frac{\Lambda c^2}{3H^2}, \quad \Omega_k \equiv \frac{-kc^2}{a^2 H^2} . \quad (1)$$

Here, $a(t)$ is the expansion factor of the universe, $H(t) \equiv \dot{a}/a$ is the Hubble constant, $\rho_m(t)$ is mean the mass density, Λ is the cosmological constant, and k is the curvature parameter. Hereafter, the above symbols for the cosmological parameters refer to their values at the present time, t_0 .

We denote $\Omega_{tot} \equiv \Omega_m + \Omega_\Lambda$, which by Eq. 1 equals $1 - \Omega_k$; its value relative to unity determines whether the universe is open ($k = -1$), flat ($k = 0$), or closed ($k = +1$). Another quantity of interest is the deceleration parameter, $q_0 \equiv -a\ddot{a}/\dot{a}^2$, which by Eq. 1 is related to the other parameters via $q_0 = \Omega_m/2 - \Omega_\Lambda$.

The FRW model also predicts a relation between the dimensionless product $H_0 t_0$ and the parameters Ω_m and Ω_Λ . For $\Omega_\Lambda = 0$, this product ranges between 1 and $2/3$ for Ω_m in the range 0 to 1 respectively, and it is computable for any values of Ω_m and Ω_Λ (§2.5).

The global measures commonly involve combinations of the cosmological parameters. Constraints in the $\Omega_m - \Omega_\Lambda$ plane are displayed in Figure 1.

2.1 Occam’s Razor

The above working hypotheses, and the order by which more specific models should be considered against observations, are guided by the principle of Occam’s Razor, *i.e.*, by simplicity and robustness to initial conditions. The caveat is that different researchers might disagree on the evaluation of “simplicity”.

It is commonly assumed that the simplest model is the Einstein-deSitter model, $\Omega_m = 1$ and $\Omega_\Lambda = 0$. One property that makes it robust is the fact that Ω_m remains constant at all times with no need for fine tuning at the initial conditions (the “coincidence” argument [2]).

The most natural extension according to the generic model of inflation is a flat universe, $\Omega_{tot} = 1$, where Ω_m can be smaller than unity but only at the expense of a nonzero cosmological constant.

These simple models could serve as useful references, and even guide the interpretation of the results, but they should not bias the measurements.

2.2 Classical Tests of Geometry

The parameter-dependent large-scale geometry of space-time is reflected in the volume-redshift relation. There are two classical versions of the tests that utilize this dependence:

magnitude versus redshift (or “Hubble diagram”) and number density versus redshift. The luminosity distance to a redshift z , which enters the Hubble diagram test, depends on Ω_m and Ω_Λ via the integral (e.g., [1])

$$d_l(z) = \frac{c(1+z)}{H_0|\Omega_k|^{1/2}} S_k \left[|\Omega_k|^{1/2} \int_0^z F(\Omega_m, \Omega_\Lambda, z') dz' \right],$$

$$F(\Omega_m, \Omega_\Lambda, z) \equiv [(1+z)^2(1+\Omega_m z) - z(2+z)\Omega_\Lambda]^{-1/2}, \quad (2)$$

where $S_0(x) \equiv x$, $S_{+1} \equiv \sin$ and $S_{-1} \equiv \sinh$. At $z \sim 0.4$, d_l happens to be (to a good approximation) a function of the combination $\Omega_m - \Omega_\Lambda$ (not q_0) [3]. The angular diameter distance, which enters the tests based on number density, is simply $d_a = d_l/(1+z)^2$.

New Developments: Accumulating data of supernovae type Ia (SNIa) out to $z \sim 0.4$ and beyond look promising for a Hubble-diagram test [3]. The preliminary success of the method may indicate that it will be able to separate the dependences on Ω_m and Ω_Λ within a few years, once several supernovae are measured at $z \sim 1$ [4]. • Measurements of the galaxy number count $N(m, z)$ seem to be in reach for surveys at high redshift [5].

Pro: The main advantage of such tests is that they are direct measures of global geometry and thus independent of assumptions regarding the mass type and distribution, the statistical nature of the fluctuations, the growth by gravitational instability (GI) and galaxy biasing. • The galaxy-type “standard candles” that were used over the years clearly suffer from severe evolution complications. Supernovae type Ia are the popular current candidate for a standard candle, based on the assumption that stellar processes are not likely to vary much in time. • Systematic searches for supernovae are in progress.

Con: The key question is whether SNIa are indeed a standard candle. Some caution is in place as long as we lack a complete theory for supernovae. If they are exploding white dwarfs, perhaps the generic SNIa at $z \sim 1$ comes from a higher mass white dwarf than one does today? • Luminosity density distributions also have to assume how galaxies evolve. If galaxies are formed in a series of hierarchical mergers that continues at low levels today, there will be more galaxies in the past than now, requiring an accurate theory of galaxy merging to deduce an accurate estimate of density evolution linked to cosmology.

Current Results: The first 7 supernovae analyzed by Perlmutter *et al.* [3] at $z \sim 0.4$ yield $-0.3 < \Omega_m - \Omega_\Lambda < 2.5$ as the 90% two-parameter likelihood contour (Fig. 1). For a *flat* universe they find for each parameter $\Omega_m = 0.94_{-0.28}^{+0.34}$, and $\Omega_\Lambda < 0.51$ (or $\Omega_m > 0.49$) at 95% confidence. Improved results are expected soon from tens of supernovae. • So far, the galaxy number counts from the Hubble Space Telescope (HST) and the 10-meter Keck telescope still yield conflicting results (see a summary in [6]).

2.3 Number Count of Quasar Lensing

This is a promising new version of the classical number density test. Strong sensitivity to Ω_Λ arises when Ω_Λ is positive and comparable to Ω_m . In this case, the universe should have gone through a phase of slower expansion in the recent cosmological past, which should be observed as an accumulation of objects at a specific redshift of order unity. In particular, it should be reflected in the observed rate of lensing of high-redshift quasars by foreground galaxies [7]. The probability of lensing of a source at redshift z_s by a population of isothermal

spheres of constant comoving density as a function of the cosmological parameters is [1]:

$$P_{lens} \propto \int_0^{z_s} (1+z)^2 F(\Omega_m, \Omega_\Lambda, z) [d_a(0, z)d_a(z, z_s)/d_a(0, z_s)]^2 dz , \quad (3)$$

where $d_a(z_1, z_2)$ is the angular diameter distance from z_1 to z_2 . The contours of constant lensing probability in the $\Omega_m - \Omega_\Lambda$ plane for $z_s \sim 2$ [1] happen to almost coincide with the lines $\Omega_m - \Omega_\Lambda = const$. The limits from lensing are thus similar in nature to the limits from SNIa.

Pro: This test shares all the advantages of direct geometrical measures, *e.g.*, being independent of dark matter, fluctuations, GI and galaxy biasing. The high redshifts involved bring about a unique sensitivity to Ω_Λ , compared to the negligible effect that Ω_Λ has on the structure observed at $z \ll 1$.

Con: The constraint is weakened if the lensed images are obscured by dust in the early-type galaxies that are responsible for the lensing, especially if E galaxies at $z \sim 1$ have much more dust than low-redshift ones [8]. There is no clear evidence for a strong effect. • A similar uncertainty arises if these galaxies had rapid evolution between $z \sim 1$ and the present; current evidence suggests a weak evolution. • The method was criticized for its sensitivity to the velocity dispersion assumed for the typical lenses and thus to the galaxy luminosity function [9], but the requirement that the distribution of lenses should simultaneously produce the observed distribution of image separations largely invalidates this criticism [10].

Current Results: From the failure to detect the accumulation of lenses, the current limit for a *flat* model is $\Omega_\Lambda < 0.66$ (or $\Omega_m > 0.36$) at 95% confidence [10] (Fig. 1). If $\Omega_\Lambda = 0$, this test provides only a weaker bound, $\Omega_m > 0.2$ at 90% confidence. Several new lenses are found each year, promising slow but continuous improvement.

2.4 Microwave Background Acoustic Peaks

This is the most promising test. In less than a decade it is expected to provide the most stringent constraints on the cosmological parameters. The test uses the effect of the background cosmology on the geodesics of photons. Current ground-based and balloon-born experiments already provide preliminary constraints on the *location* of the first acoustic peak on sub-degree scales in the angular power spectrum of CMB temperature fluctuations, $l(l+1)C_l$. The dependence of the peak location on the cosmological parameters enters via the combined effect of (a) the physical scale of the “sound horizon” that is proportional to the cosmological horizon at recombination, and (b) the geometry of space-time via the angular-diameter distance. In the vicinity of a flat model, the first peak is predicted at approximately the multipole (*e.g.*, [11] [12])

$$l_{peak} \simeq 220(\Omega_m + \Omega_\Lambda)^{-1/2}. \quad (4)$$

New Developments: The next generation of post-COBE CMB satellites (MAP to be launched by NASA in 2001, and in particular COBRAS/SAMBA scheduled by ESA for 2004) are planned to obtain a precision at ~ 10 arc-minute resolution that will either rule out the current framework of GI for structure formation or will measure the cosmological parameters to high precision. Detailed evaluation of COBRAS/SAMBA shows that nominal performance and expected foreground subtraction noise will allow parameter estimation with the following accuracy: $H_0 \pm 1\%$, $\Omega_{tot} \pm 0.005$, $\Omega_\Lambda \pm 0.02$, $\Omega_b \pm 2\%$.

Pro: The precision hoped for is much better than attainable with any other known method. If the observations fit the model, the precision is such that the model will be confirmed beyond reasonable doubt. • The constraints on Ω_{tot} come mostly from geometrical effects. The interpretation is based on well understood physics of sound waves in the linear regime, and on the assumption of absence of any relevant preferred scale (in the megaparsecs to gigaparsec range) in the physics which generated the initial structure. The latter assumption can be checked directly by the observations themselves.

Con: The measurements might be messed up by unexpected foreground contamination (*e.g.*, by diffuse matter in galaxy groups). • The detailed measurements need to wait 5 to 10 years. • The assumption of no preferred scale in the initial fluctuations may be wrong. • If the observations do not fit the model, the whole paradigm behind current structure formation modeling will be excluded, and then no parameter estimates will be possible. However, this seems unlikely given the recent measurements from the ground and from balloons, which have already confirmed the existence of the first acoustic peak.

Current Results: Balloon and ground-based results have already confirmed the existence of the first acoustic peak, and have constrained its location to the vicinity $l \sim 200$. The results of COBE's DMR ($l \sim 10$) provide an upper bound of $\Omega_m + \Omega_\Lambda < 1.5$ at the 95% confidence level for a scale-invariant initial spectrum (and the constraint becomes tighter for any "redder" spectrum, $n < 1$) [12]. Several balloon experiments ($l \sim 50 - 200$) strengthen this upper bound [13]. The CAT experiment ($l \sim 350 - 700$) yields a preliminary lower bound of $\Omega_m + \Omega_\Lambda > 0.3$ [14] (Fig. 1).

2.5 The Age of the Universe

Measured independent lower bounds on the Hubble constant and on the age of the oldest globular clusters provide a lower bound on $H_0 t_0$ ($= 1.05ht$, where $H_0 \equiv 100h \text{ km s}^{-1} \text{ Mpc}^{-1}$ and $t_0 \equiv 10t \text{ Gyr}$), and thus an interesting constraint in the $\Omega_m - \Omega_\Lambda$ plane. The exact expressions are computable in the various regions of parameter space. For example, for $\Omega_\Lambda = 0$, the relation is (*e.g.*, [15], Eq. 2.79)

$$H_0 t_0 = \frac{1}{2} \frac{\Omega_m}{|1 - \Omega_m|^{3/2}} k \left[C_k^{-1} \left(\frac{2}{\Omega_m} - 1 \right) - \frac{2|1 - \Omega_m|^{1/2}}{\Omega_m} \right], \quad (5)$$

where $C_{+1}^{-1} \equiv \cos^{-1}$ and $C_{-1}^{-1} \equiv \cosh^{-1}$. A very useful approximation in the presence of a cosmological constant, that is an exact solution for a flat universe, is [1]

$$H_0 t_0 = \frac{2}{3} \frac{1}{|1 - \Omega_a|^{1/2}} S_a^{-1} \left(\frac{|1 - \Omega_a|^{1/2}}{\Omega_a^{1/2}} \right), \quad \Omega_a \equiv 0.7\Omega_m - 0.3\Omega_\Lambda + 0.3, \quad (6)$$

where $S_{\Omega_a \leq 1}^{-1} \equiv \sinh^{-1}$ and $S_{\Omega_a > 1}^{-1} \equiv \sin^{-1}$. A useful crude approximation near $H_0 t_0 \sim 2/3$ is

$$\Omega_m - 0.7\Omega_\Lambda \simeq 5.8(1 - 1.3ht). \quad (7)$$

New Developments: Progress is being made in the HST key project to measure H_0 based on Cepheids in Virgo and Fornax.

Pro: The method does not depend on fluctuations, GI, biasing, etc. • The current error of $\sim 20\%$ in the Hubble constant will hopefully be reduced soon to the level of 10% percent.

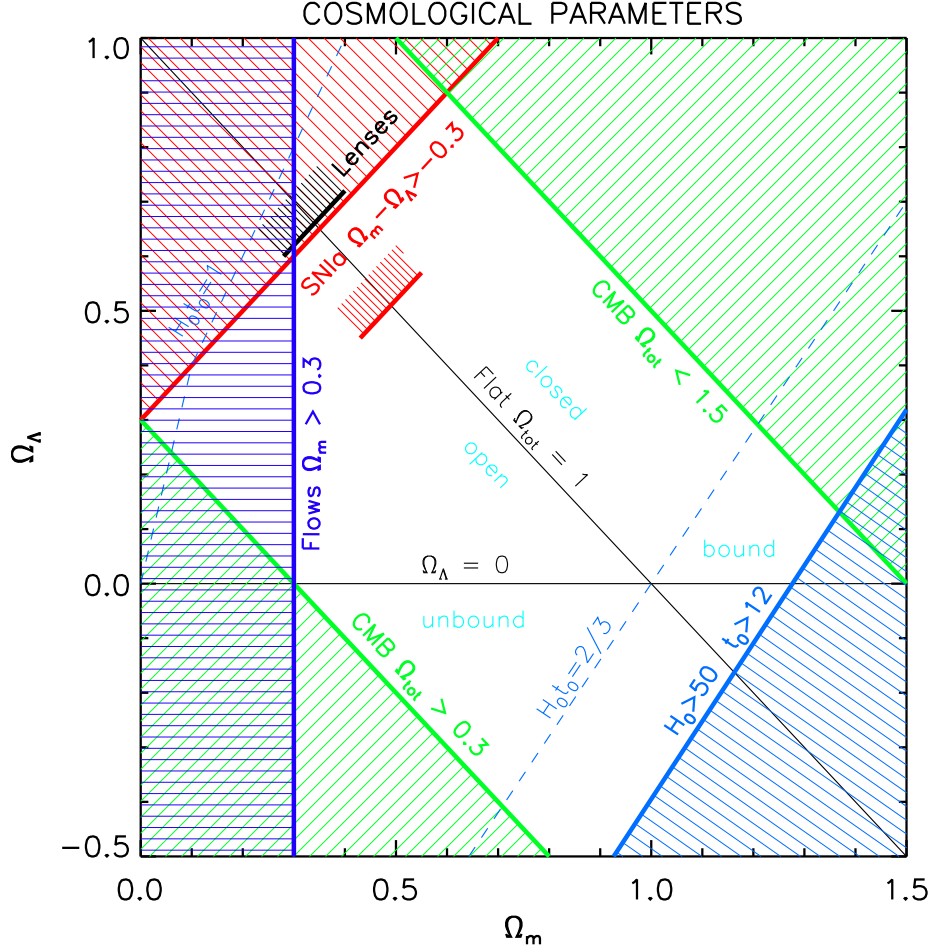


Figure 1: Current limits ($\sim 2\sigma$) on the cosmological parameters Ω_m and Ω_Λ from global measures: luminosity distance of SNIa, lens count, the location of the CMB peak, and the age versus Hubble constant. The short marks are the one-parameter 95% limits from SNIa and lenses for a flat universe. Also shown (vertical line) is the 95% lower bound on Ω_m from cosmic flows. The most likely value of Ω_m lies in the range 0.5 to 1. The Einstein-deSitter model is permitted. An open model with $\Omega_m \simeq 0.2$ and $\Omega_\Lambda = 0$, or a flat model with $\Omega_m \simeq 0.3$ and $\Omega_\Lambda \simeq 0.7$, are ruled out.

- This method is likely to provide the most stringent upper bound on Ω_m and lower bound on Ω_Λ .

Con: The errors in the determination of the age of the universe based on globular clusters are uncertain. The major source of error are the distances to Pop-II stars in the globular clusters, and complex stellar evolution issues.

Current Results: The most likely estimates are of $h \simeq 0.6 - 0.7$ [16] and $t \simeq 1.5$ [17], corresponding to $ht \simeq 1$. They seem to favor a possible deviation from the Einstein deSitter model towards low Ω_m or high Ω_Λ or both. However, one only needs to appeal to the current $\sim 1\sigma$ lower bounds (say $h \simeq 0.53$ and $t \simeq 1.2$) in order to accommodate the Einstein deSitter model.

Figure 1 displays in the Ω_m - Ω_Λ plane the \sim two-sigma constraints from the global mea-

tures discussed above. Superposed is the main constraint from cosmic flows (§4 below). The joint permitted range for Ω_m is thus roughly 0.4 to 1.1. Low Ω_m models of $\Omega_m \leq 0.3$ are significantly ruled out.

3 Virialized Objects: Galaxies and Clusters

These methods measure the mass associated with galaxies and clusters on scales of order one to a few $h^{-1}\text{Mpc}$. The structure is assumed to have grown from small initial fluctuations via GI, and the methods involve nonlinear dynamics of virialized systems. The cosmological constant is irrelevant; the structure at low redshift is insensitive to Ω_Λ .

Several additional physical quantities are now involved, such as the baryonic contribution to the universal mass density, Ω_b . The complex relation between galaxies and mass, termed “biasing”, enters as a crucial unknown on these galactic scales, and issues of gas dynamics are important. These complications introduce severe uncertainties into the estimates of Ω_m .

3.1 Mass to Light Ratio

The mass-to-light ratio M/L is measured from virialized systems from galaxies up to rich clusters. The asymptotic universal value of the luminosity density, \mathcal{L} , is estimated by integrating the galaxy luminosity function. The mass-to-light ratio in clusters is assumed to be the same as outside clusters. Then

$$\Omega_m = 0.33 \left(\frac{M/L}{300hM_\odot/L_\odot} \right) \left(\frac{\mathcal{L}}{3 \times 10^8 h L_\odot \text{ Mpc}^{-3}} \right). \quad (8)$$

New Developments: Better masses for clusters and groups are now available from virial analysis of galaxies, from X-ray gas with resolved temperature structure, and from gravitational lensing. • Masses for extended galaxy halos are also becoming available from satellite galaxies and from lensing.

Pro: This is a simple, straightforward method. The result is independent of H_0 .

Con: The basic hypothesis is unjustified. It rests on the implicit assumption that galaxies form in an unbiased way. Clusters and groups may have extended dark halos that are not traced by the galaxies or by the X-ray gas, so M/L may vary within the clusters as a function of radius. This problem is even worse within galactic halos. • The total mass of clusters may be underestimated in the virial analysis based on galaxy velocities because of possible velocity antibiasing, and because of applying a spherical analysis to elongated systems. • The mass based on X-ray measurements may be underestimated by the assumption that the X-ray gas is in hydrostatic equilibrium. The data allows significant freedom in the mass profile, which translates to an uncertainty of factor two within the Abell radius, and a larger error at larger radii [18]. • The luminosity density may not be contributed by the same stars that dominate the cluster light. There are factors of 2-3 uncertainties in \mathcal{L} stemming, for example, by differences in overall metallicity and extinction by dust.

Current Results: From virial analysis of galaxy velocity dispersions in several clusters stuck together, and a corresponding estimate of \mathcal{L} : $\Omega_m \simeq 0.25 \pm 0.05$ [19].

3.2 Baryon Fraction and Nucleosynthesis

The baryon fraction in clusters, f_b , is assumed to be equal to the cosmic value. Combined with the universal baryon density Ω_b as predicted from light element abundances through the theory of big-bang nucleosynthesis (BBN) it yields the cosmic mass density [20]:

$$\Omega_m = (\Omega_b/0.1)(f_b/0.1)^{-1}. \quad (9)$$

New Developments: The baryonic content is mostly in the form of X-ray gas, and is estimated from ROSAT to large radii. The reliability of the gas mass estimates is partly confirmed by (a) direct spectral limits on gas inhomogeneity, and (b) limits on the cluster magnetic fields from Faraday rotation of background sources. Independent cluster masses are obtained from gravitational lensing. • The Deuterium abundance is being measured from quasar absorption systems that are assumed to be composed of unprocessed primordial material.

Pro: This method avoids assumptions about galaxy biasing and stellar populations; it depends on the relatively safe assumption that cluster formation proceeds by collapse from a well mixed medium, and the assertion that only little segregation occurred between the gas and the dark matter.

Con: The baryonic mass could be overestimated if the X-ray gas is locally inhomogeneous, or if large tangled magnetic fields provide a significant part of the pressure in cluster centers. • The total mass of clusters may be underestimated as in the M/L method. • The baryon fraction seems to increase with cluster mass and sometimes with radius within a cluster. Plausible physical processes eject gas from the inner regions of lower mass systems, making f_b an underestimate of the global baryon fraction, and leading to an overestimate of Ω_m . The method assumes that the baryonic fraction in clusters is equal to the universal value even though clusters only contain a few percent of the galaxies in the universe. • The method relies on the uncertain interpretation of the light element abundances and on the theory of big-bang nucleosynthesis.

Current Results: The baryonic fraction is estimated to be in the range $f_b = (0.03 - 0.08)h^{-3/2}$ by [21], but has also been estimated to have a factor of 5 range among galaxy groups and clusters of similar mass [22]. The larger values typically apply to the most massive and best observed clusters, but preliminary ASCA results indicate lower values in several rich clusters. Low values are also indicated in groups [23]. • The current BBN results suffer from uncertainty in the primordial Deuterium abundance. The traditional estimates are of low Ω_b , e.g., of $0.009 \leq \Omega_b h^2 \leq 0.02$ based on all the light elements, and $0.006 \leq \Omega_b h^2 \leq 0.03$ from Deuterium only [24]. Recent, high-resolution spectra from the Keck telescope show a lower Deuterium abundance in two quasar absorption systems that seem to consist of unprocessed primordial material, and correspondingly $\Omega_b h^2 = 0.024_{-0.005}^{+0.006}$ [25].

With f_b in the middle of the range quoted above, the estimate is either $\Omega_m \simeq 0.3h_{65}^{-1/2}$ (for low Ω_b) or $\Omega_m \simeq 0.55h_{65}^{-1/2}$ (for high Ω_b), but in either case $\Omega_m = 1$ cannot be definitively excluded.

3.3 Cosmic Virial Theorem

In the cosmic virial theorem (CVT), clustering is assumed to be statistically stable on scales $\gtrsim 1 h^{-1}\text{Mpc}$, such that the ensemble-average contribution of a third mass particle to the

relative acceleration of a pair of galaxies is balanced by the relative motions of the ensemble of pairs. The kinetic energy is represented by the pairwise relative velocity dispersion of galaxies [$\sigma_{12}(r)$], and the potential energy involves a combination of integrals of the 2- and 3-point galaxy correlation functions [26]. A very crude approximation to the actual relation is

$$\sigma_{12}^2(r) = \Omega_m \xi(r) r^2, \quad (10)$$

where $\xi(r)$ is the two-point correlation function. In some ways this is like stacking many groups of galaxies to get a mean M/L , so it can be regarded as a statistical version of the mass-to-light ratio method.

On scales $1 - 10 h^{-1}\text{Mpc}$ the more useful statistics for dynamical mass estimates is the mean (first moment) pairwise velocity in comparison with an integral of the galaxy two-point correlation function.

In the approach of the Layzer-Irvine (LI) equation, the kinetic energy is associated with the absolute rms velocity (in the CMB frame) of individual galaxies and the potential energy is an integral over the 2-point correlation function.

New developments: It has been realized that the pair velocity dispersion is an unstable statistic that is dominated by galaxies in clusters. Attempts are being made to apply the method while excluding clusters. • Filtered versions of the LI approach help truncate the (weak) divergence in estimating the potential energy and make the kinetic energy term easier to estimate from data.

Pro: There is no need to associate galaxies with separate groups and clusters; it is all statistical. • In the LI method the energies are dominated by contributions from the large-scale mass distribution, and it is therefore less contaminated by clusters and less biased by the assumption of point masses. The two-point correlation for the LI method can be measured with reasonable accuracy.

Con: The relevant correlation integrals, and in particular the 3-point correlation function that enters the CVT, are very difficult to measure. • The pair velocity dispersion in the CVT is an unstable statistic, that is dominated by pairs of galaxies in clusters. A robust, self-consistent way to avoid the clusters is yet to be found. • The absolute velocity dispersion which enters the LI equation is hard to measure. • The CVT assumes that galaxies are point masses (or of finite size), which overestimates the force that they exert, and biases Ω_m low. The overlap of extended galactic halos makes a significant difference. • The methods depend on the assumption that the statistical distribution of galaxies and mass are similar (as in the M/L method). Otherwise, they must refer to a specific model for galaxy biasing.

Current Results: The line-of-sight pair velocity dispersion outside of clusters is in the range $\sigma_f \simeq 300 \pm 100 \text{ km s}^{-1}$ [27] [28]. With Peebles' old estimate of the correlation functions, assuming point masses and no biasing, he obtains from the CVT $\Omega_m \simeq 0.15$ [6]. • From the mean pairwise velocity in IRAS 1.2Jy [27]: $\Omega_m \sim 0.25$. • However, it has been demonstrated that with an extended mass distribution in galactic halos the above CVT estimates are lower bounds, and that the observations may be consistent with $\Omega_m \simeq 1$ [29].

3.4 Local Group Dynamics

The mixed-boundary problem of a cosmological gravitating system is solved for the trajectories of galaxies in the Local Group. It is done using the least-action principle, under the

assumption that the mass is concentrated around the galaxies (*i.e.*, strict no biasing).

New Developments: Simulations are being used to estimate the biases in the method.

Pro: This method is making use of accurate local measurements.

Con: The assumption that the mass is all in point-like galaxies during the whole evolution of the Local Group is likely to be wrong, especially if Ω_m is high. It causes an overestimate of the forces and thus an underestimate of Ω_m . This is a stronger assumption than assuming no biasing in the statistical sense, $b = 1$. A related problem is the neglect of possible merging that has taken place among the initial subsystems in the Local Group. • The solution to the mixed-boundary problem may be non-unique. • The method treats the Local Group as an isolated system and neglects possible tidal effects from external material.

Current Results: Peebles [30] obtains $\Omega_m \sim 0.15$, under the assumption that galaxies strictly trace mass. However, it has been shown using N-body simulations [31] that the assumption that the mass is all in galaxies causes an underestimate of Ω_m by a factor 4 – 5 for any true Ω_m in the range 0.2 – 1.0. Shaya *et al.* [32] obtain a similarly low value using a similar analysis inside a sphere of radius $\sim 30 h^{-1}\text{Mpc}$.

4 Large-Scale Fluctuations; Cosmic Flows

These methods use the mean motions induced by the large-scale mass distributions on scales of several megaparsecs and above. They are based on GI in the linear regime and approximate extensions into the mildly-nonlinear regime. The different matter contributions to Ω_m are relevant, such as “cold” and “hot” dark matter (see [33] for a review), but the cosmological constant is not involved. The statistical nature of the initial fluctuations has to be specified in some cases; it is commonly assumed to be a *Gaussian* random field. The initial fluctuation power spectrum is characterized by the power index n on large scales, by a specific shape (*e.g.*, as predicted by CDM theory), and by its amplitude, *e.g.*, via σ_8 , the *rms* fluctuation in top-hat spheres of radius $8 h^{-1}\text{Mpc}$. Galaxy *biasing* is expected to enter in a simpler manner on these larger scales, but is still an important unknown. In the common simplified treatments it is modeled as a linear biasing relation between the density fluctuations of galaxies and mass, $\delta_g = b\delta$, with different biasing parameters for different galaxy types: b_{iras} , b_{opt} , etc. However, non-trivial properties of the biasing scheme may be important.

4.1 Measured Peculiar Velocities

These methods use data that include both redshifts and redshift-independent distances to galaxies via POTENT-like reconstructions of the underlying velocity and mass-density fields [34], independently of whole-sky redshift surveys. Combined with the assumption of Gaussian initial fluctuations, these methods provide lower bounds on Ω_m in various ways [35], such as (a) using the fact that diverging flows in voids cannot be large when Ω_m is low because the voids cannot be more empty than empty [36], (b) using the skewness of $\nabla \cdot \mathbf{v}$ as induced by Ω_m -dependent nonlinear gravity [37], and (c) appealing to the mass-density initial probability distribution function via a Zel’dovich “time machine” [38].

New developments: The Mark III catalog of Tully-Fisher and $D_n - \sigma$ peculiar velocities with more than 3000 galaxies has been completed [39], and several new samples are coming up soon. • New, more accurate distance indicators are being developed and implemented to

larger samples. Most promising are the methods based on surface-brightness fluctuations for nearby galaxies, and supernovae type Ia for large-scale coverage ([40] for a review). • The understanding of the systematic biases in the data and the analysis is improving, and new methods for correcting them are being developed.

Pro: These methods allow direct dynamical measures of Ω_m independent of galaxy density biasing.

Con: The measurement of redshift-independent distances involves large errors that grow in proportion to distance, and the analysis is therefore limited to the relatively local cosmological volume, out to $\sim 100 h^{-1}\text{Mpc}$ in the best cases. The associated cosmic scatter is inevitably large. • Some of the distance indicators may be subject to systematic environmental effects that are hard to identify. • These methods ignore possible velocity biasing. • The methods assume potential flow and Gaussian initial conditions. These are valid hypotheses for the standard scenarios of structure formations, but they might be invalid in more esoteric models, such as those based on topological defects as seeds for structure formation.

Current Results: From Mark III peculiar velocities using several methods: $\Omega_m > 0.3$ at more than 95% confidence (reviews: [35]). From the extracted mass power spectrum under the general CDM family of models [41]: $\sigma_8\Omega_m^{0.6} = 0.8 \pm 0.2$.

4.2 Redshift Distortions

This is a statistical measure of large-scale peculiar velocities from extended redshift surveys alone, under the assumption of global isotropy in real space and linear biasing. The comparison of radial and angular fluctuations yields a measure of $\beta \equiv \Omega_m^{0.6}/b$. There are several ways to implement this idea, using correlation functions, power spectra, or expansion in spherical harmonics and Bessel functions (reviews: [35] [42]).

New developments: Redshift surveys larger than before have become available, for example PSCZ from IRAS to a flux limit of 0.6 Jy, and the Las Campanas Redshift Survey of optical galaxies in the south. Even larger surveys are planned for the next few years, such as the Two-Degree Field (2DF) and the Sloan Digital Sky Survey (SDSS) (see [43]). These catalogs will drastically reduce the cosmic scatter.

Pro: Measurements of redshifts are inexpensive; there is no need for independent distances. One can therefore use surveys of large volumes in order to beat the measurement errors and the cosmic scatter.

Con: In the mildly-nonlinear regime where the interpretation of distortions is straightforward, the noise in the observations [*e.g.*, the $\xi(\sigma, \pi)$ diagram] is bad and difficult to quantify. • With current data, the estimate suffers from large cosmic scatter. • The method is subject to galaxy density biasing. At best it measures the bias-contaminated parameter β , not Ω_m . The β estimated by this method may be systematically different from the β estimated by other methods [44].

Current Results: The best estimates for IRAS galaxies span a large range: $0.5 \leq \beta_l \leq 1.2$ [43]. The current samples do not yet probe a sufficiently fair volume of the universe, and there are indications for systematic effects near the flux limit.

4.3 Velocity versus Density

The peculiar velocity data is compared with the distribution of galaxies in redshift space to obtain β . The comparison can be performed either at the density level (*e.g.*, velocity-inferred mass density a la POTENT versus real-space density of galaxies as extracted from redshift surveys [45]), or at the velocity level [46] [47], or simultaneously [48] (reviews: [35] [42]).

New developments: The methods are being improved to better take into account the random and systematic errors. The comparison is done in several different ways.

Pro: Some of the comparison methods allow a direct mapping of the biasing field. • Certain versions of the method are straightforward to implement.

Con: It is hard to impose the same effective smoothing on the two data sets. This may cause a bias in the estimate of β , and a complication due to possible scale dependence in the biasing scheme. • The estimation is contaminated by the possible complexity of the biasing scheme. Each method may actually refer to a somewhat different β [44]. • It is hard to distinguish nonlinear biasing from nonlinear gravitational effects.

Current Results: For IRAS galaxies, the current best estimates vary in the range $0.5 \leq \beta_I \leq 1.2$, depending on the method, the volume used, the weighting of the different data, the smoothing scale, etc. The comparisons at the density level [45] tend to yield higher estimates than the comparisons at the velocity level [46]. One of the velocity comparisons indicates a possible inconsistency in the data at large distances [47]. The value of β_I seems to grow with smoothing scale, from $\beta_I \sim 0.5 - 0.6$ at Gaussian smoothing scales of $3 - 6 h^{-1}\text{Mpc}$ [46] [48] to $\beta_I \sim 1$ on scales of $\sim 12 h^{-1}\text{Mpc}$ [45] [48]. The estimates for optical galaxies indicate a biasing parameter that is typically larger by $\sim 30\%$.

4.4 Cluster Abundance and Correlations

If clusters can be modeled (*e.g.*, using an improved version of the Press-Schechter formalism) as “objects” above a mass threshold in a density fluctuation field that was initially Gaussian, then the cluster mass function can be used to constrain $\sigma_8 \Omega_m^{0.6}$ [49]. The correlation amplitude of these clusters can be compared with their abundance to give a direct measure of σ_8 . Together, these results yield Ω_m and σ_8 separately [50].

Pro: The two parameters are determined from observational data that are relatively easy to obtain. • The method depends sensitively only on the assumptions of Gaussian statistics and of mass-limited cluster definition. It is insensitive to the actual power spectrum of fluctuations.

Con: The amplitude of cluster correlations still carries a large uncertainty. • The method relies on the assumption of Gaussian initial conditions.

Current Results: $\sigma_8 \Omega_m^{0.6} \simeq 0.5 - 0.6$ [49] from cluster abundances (compare to §4.1), but measures of the cluster autocorrelation strength are still too uncertain to be able to give a useful second constraint [50].

5 Fluctuation Growth Rate

The amplitude of density fluctuations at redshift z compared to their amplitude today, according to linear GI theory, is approximated to a few percent by [51]

$$\delta \simeq (1+z)^{-1} 2.5 \Omega_m [\Omega_m^{4/7} - \Omega_\Lambda + (1 + \Omega_m/2)(1 + \Omega_\Lambda/70)]^{-1} . \quad (11)$$

A main discriminatory feature between low- Ω_m and high- Ω_m models is the effective freeze-out of the growth of fluctuations, which occurs when the universe enters its free expansion phase; roughly at $1+z \sim \Omega_m^{-1}$ in an open model with $\Omega_\Lambda = 0$, or later at $1+z \sim \Omega_m^{-1/3}$ in a low density flat universe with a cosmological constant. Thus, structure of a given amplitude today form earlier in low- Ω_m models than in $\Omega_m = 1$ models, and more so in an open model than in a flat model. This effect can be observed in several different ways.

5.1 Cluster Morphology

Clusters are expected to be more evolved in a low- Ω_m universe, *i.e.*, be more spherical and show less substructure than clusters in an $\Omega_m = 1$ universe which must still be undergoing significant collapse and merger activity [52].

New Developments: X-ray maps from ROSAT provide a useful measure of morphology for many clusters.

Pro: The method relies on a simple feature distinguishing the different cosmologies by the rate of evolution of structure at different epochs. Qualitative results can be obtained by visual inspection of maps.

Con: The method requires high-resolution simulations with gas dynamics and many clusters in order to beat the cosmic scatter. • Substructure is hard to quantify. • The substructure depends also on the fluctuation power spectrum, on Ω_b , and on the various other dark matter species.

Current Results: Dissipative simulations [53] agree with dissipationless simulations [54] that a significant effect is expected. However, these papers disagree about its strength and about the conclusions to be drawn from comparison with the clusters observed by ROSAT. The current situation is somewhat confused.

5.2 The Epoch of Galaxy Formation

Can the observed number count $N(z)$ at high z (of a few) be compatible with $\Omega_m = 1$? This test can involve various objects such as quasars, early galaxies, damped Lyman alpha systems. etc.

New Developments: There are HST and Keck observations of central regions of galaxies in an early stage of their formation at $z \sim 3 - 3.5$ (some claim that galaxies are observed all the way to $z \sim 6$ based on “photometric redshifts”). Improved spectrographs are being developed, as well as methods for estimating “photometric redshifts”.

Pro: New data are accumulating rapidly from HST and 8-10 meter telescopes.

Con: The method is contaminated by unknown evolutionary issues. • The model predictions depend on the power spectrum of fluctuations. • Dissipationless simulations predict the number density of halos $N(M, z)$, but not necessarily of luminous objects.

Current Results: The number count of quasars may be consistent with $\Omega_m = 1$ provided that there was efficient cooling and angular-momentum transfer [55]. • The abundance of bright galaxies seen at $z \sim 3.5$ [56] may favor low Ω_m [57]. On the other hand, the relatively small number of galaxies identified in the Hubble Deep Field with colors consistent with very high redshifts ($z = 4 - 6$) [58] may indicate that low Ω_m values can be excluded.

5.3 Present Structure versus Fluctuations in the CMB

This method is using independent constraints on the power spectrum of today’s fluctuations on scales $\sim 100 h^{-1}\text{Mpc}$, and the power spectrum of fluctuations at $z \sim 10^3$ on scales $100 - 1000 h^{-1}\text{Mpc}$, assuming gravitational growth.

New Developments: Peculiar velocity data enable constraints on Ω_m independent of biasing. Future extended redshift surveys (2DF, SDSS) will provide constraints on $> 100 h^{-1}\text{Mpc}$ scales. COBE data put limits on scales $\sim 1000 h^{-1}\text{Mpc}$. Accumulating ground-based and balloon data of CMB fluctuations with sub-degree resolution start providing constraints on scales $\sim 100 h^{-1}\text{Mpc}$.

Pro: With peculiar velocity data this method compares measures of dynamical fluctuation fields independent of galaxy biasing.

Con: As long as the scales explored by today’s structure and the CMB fluctuations do not overlap, the constraint on Ω_m depends on n . • A hot dark matter component would alter the result via a different fluctuation growth rate, and confuse the constraints. • If today’s power spectrum is extracted from a galaxy redshift survey then the method depends on galaxy biasing on large scales.

Current Results: Using COBE and Mark III velocities, and considering the family of Inflation-motivated CDM models with a possible cosmological constant such that $\Omega_m + \Omega_\Lambda = 1$ and a possible tilt in the initial power spectrum, a likelihood analysis yields: $\Omega_m h_{65} n^2 = 0.7 \pm 0.1$ [41]. The best fit for CDM is thus obtained with a slight deviation from the “standard” CDM model, of either $n \sim 0.8 - 0.9$, $\Omega_m \sim 0.7$, or $\Omega_\nu \sim 0.2$. The indicated height of the first acoustic peak of the CMB allows only a slight tilt, $n \sim 0.9$, and a high baryon content, $\Omega_b \sim 0.1$ [59].

6 Conclusion

Table 1 summarizes the current estimates of Ω_m from the various methods of measurement. In general, the methods based on virialized objects favor low values, while the global measures (with the exception of the age argument) and the analysis of large-scale structure and flows tend towards higher values. The estimates that indicate very low values ($\sim 0.1 - 0.2$) have plausible loopholes. On the other hand, none of the estimates that favor high Ω_m values actually requires that Ω_m is as large as unity. It thus seems that a tentative consensus can be reached at a (not very elegant) value of about $\Omega_m \simeq 0.5$. This was reflected in the debate on formation scenarios by the fact that the competing CDM models were the Einstein deSitter $\Omega_m = 1$ “standard” CDM (with $n \sim 0.9$) or Hot+CDM, versus the Open CDM and Flat (Λ) CDM models with $\Omega_m \simeq 0.4$. Not too long ago these low- Ω_m models used to be associated with $\Omega_m \sim 0.1 - 0.2$. It seems that progress is being made towards convergence. The activity on many fronts of this field promises that we will know more in the near future. We hope

that the above discussion will be of help in the effort to reconcile the various estimates with a unique value of Ω_m .

Table 1: Estimates of Ω_m

Global Measures	Inflation, Occam	$\Omega_m + \Omega_\Lambda = 1$ ($\Omega_m = 1, \Omega_\Lambda = 0$)
	Lum. distance SNIa	$-0.3 < \Omega_m - \Omega_\Lambda < 2.5$ (90%)
		Flat $\Omega_m > 0.49$ (95%)
	Lens Counts	Flat $\Omega_m > 0.34$ (95%)
	CMB Peak	$\Omega_m + \Omega_\Lambda < 1.5$ (95%)
		$\Omega_m + \Omega_\Lambda > 0.3$ (likely ~ 0.7)
	$H_0 t_0$	$\Omega_m - 0.7\Omega_\Lambda < 1.3$ (likely ≤ 0)
Virialized Objects	$(M/L)\mathcal{L}$	$\Omega_m \sim 0.25$ (0.1 – 1.0)
	Baryon fraction	$\Omega_m h_{65}^{1/2} \sim 0.3 - 0.5$ (low–high Ω_b)
	Cosmic Virial Th.	Point mass $\Omega_m \sim 0.2$ (halos $\rightarrow 1$)
	Local Group	Point mass $\Omega_m \sim 0.15$ (halos $\rightarrow 0.7$)
Large-Scale; Flows	Peculiar velocities	$\Omega_m > 0.3$ (95%)
		$\Omega_m^{0.6} \sigma_8^a = 0.8 \pm 0.2$ ($\beta_I^b \simeq 1.05^c$)
	Redshift Distortions	$\beta_I \sim 0.5 - 1.2$
	Velocity vs Density	$\beta_I \sim 0.5 - 1.2$ (scale dependent)
		$\beta_O \sim 0.4 - 0.95$
	Cluster Abundance	$\Omega_m^{0.6} \sigma_8 \simeq 0.5 - 0.6$ ($\beta_I \simeq 0.7 - 0.8^c$)
Fluct. Growth	Cluster Morphology	$\Omega_m > 0.2$ (?)
	Galaxy Formation	(?)
	$P_k(\rho)$ vs C_l	CDM $n = 1$ $b = 1$: $\Omega_m h_{65} \sim 0.3$
	$P_k(v)$ vs C_l	CDM flat: $\Omega_m h_{65} n^2 \simeq 0.7 \pm 0.1$

^a σ_8 is the *rms* mass density fluctuation in a top-hat sphere of radius $8 h^{-1}$ Mpc.

^b $\beta \equiv \Omega^{0.6}/b$, b_I for IRAS galaxies, b_O for optical galaxies.

^c $b_O/b_I \simeq 1.3$, $b_O \simeq 1/\sigma_8$.

References

- [1] Carroll, S.M, Press, W.H., & Turner, E.L. 1992, *Annu. Rev. Astron. Astrophys.* **30**, 499
- [2] Bondi, H. 1960, *Cosmology* (Cambridge University Press) p. 166
- [3] Perlmutter, S., Gabi, S., Goldhaber, G. *et al.* 1996, *Ap.J.* , submitted (astro-ph/9602122)
- [4] Goobar, A., & Perlmutter, S. 1995, *Ap.J.* **450**, 14
- [5] Lilly, S.J., Tresse, L, Hammer, F., Crampton, D., & Le Fevre, O. 1995, *Ap.J.* **455**, 108; Lilly, S.J., Le Fevre, O., Hammer, F., & Compton, D. 1996, *Ap.J.* **460**, L1
- [6] Peebles, P.J.E. 1997, in *Formation of Structure in the Universe*, eds. A. Dekel and J.P. Ostriker (Cambridge University Press), in press
- [7] Fukugita, M., Futamase, T., Kasai, M. 1990, *MNRAS* **246**, 24; Turner, E.L. 1990, *Ap.J. Lett.* **365**, L43
- [8] Malhotra, S., Rhoads, J.E., & Turner, E.L. 1997, *MNRAS* , submitted (astro-ph/9610233)
- [9] Chiba, M, & Yoshii, Y. 1996, *Ap.J.* , submitted
- [10] Kochanek, C.S. 1996, *Ap.J.* **466**, 638
- [11] White, M., Scott, D., & Silk, J. 1994, *Annu. Rev. Astron. Astrophys.* **32**, 319
- [12] White, M., & Scott, D. 1996, *Ap.J.* **459**, 415
- [13] Cheng, E.S. *et al.* 1994, *Ap.J. Lett.* **422**, L37; De Bernardis, G.B. *et al.* 1994, *Ap.J. Lett.* **422**, L33; Gundersen, J.O., Lim, M., Staren, J. *et al.* 1995, *Ap.J. Lett.* **443**, L57; Ruhl, J.E., *et al.* 1995, *Ap.J. Lett.* **453**, L1; Tanaka, S.T., Clapp, A.C., Devlin, M.J. *et al.* 1996, *Ap.J.* , in press (astro-ph/9512067); Scott P.F., Saunders, R., Pooley, G. *et al.* 1996, *Ap.J. Lett.* **461**, L1
- [14] Hancock, S., Rocha, G., Lasenby, A.N., & Cutierrez, C.M. 1996, *MNRAS* , submitted
- [15] Padmanabhan, T. 1993, *Structure Formation in the Universe* (Cambridge University Press)
- [16] Freedman, W.L. *et al.* 1994, *Nature* **371**, 757; Tanvir, N.R., Shanks, T., Ferguson, H.C., & Robinson, D.R.T. 1995, *Nature* **377**, 27; Freedman, W. 1996, this volume; Tammann, G. 1996, this volume
- [17] Stetson, P.B., van den Berg, D.A., & Bolte, M. 1996, *Proc. Ast. Soc. Pac.* **108**, 560; Van den Berg, D., Stetson, P., & Bolte, M. 1996, *Annu. Rev. Astron. Astrophys.* **34**, 461; Chaboyer, B., Demarque, P., Kernan, P.J., & Krauss, L.M. 1996, *Science* **271**, 957
- [18] Balland, C., & Blanchard, A. 1996, astro-ph/9510130
- [19] Carlberg, R.G., Yee, H.K.C., Ellingson, E., Abraham, R., Cravel, P., Morris, S., & Pritchett, C.J. 1996, *Ap.J.* **462**, 32

- [20] White, S.D.M., Navaro, J., Evrard, A., & Frenk, C.S. 1993, *Nature* **366**, 429
- [21] White, S.D.M., & Fabian, A. 1995, *MNRAS* **273**, 72
- [22] Loewenstein, M., & Mushotzky, R.F. 1996, *Ap.J. Lett.* **471**, L83; Mushotzky, R.F. 1996, in the Vatican Workshop, November 24; Gunn, K.F., & Thomas, P.A. 1996, astro-ph/9510082
- [23] Mulchaey, J.S., Davis, D.S., Mushotzky, R.F., & Burstein, D. 1996, *Ap.J.* **456**, 80
- [24] Copi, C.J., Schramm, D.N., & Turner, M.S. 1995, *Science* 267, 192; Hogan, C. 1996, this volume.
- [25] Tytler, D., Fan, X.M., & Burles, S. 1996, *Nature* **381**, 207; Burles, S., & Tytler, D. 1996, *Science*, submitted (astro-ph/9603070)
- [26] Peebles, P.J.E. 1980, *The Large-Scale Structure of the Universe* (Princeton University Press)
- [27] Fisher, K.B., Davis, M., Strauss, M.A., Yahil, A., & Huchra, J.P. 1994, *MNRAS* **267**, 927
- [28] Marzke, R.O., Geller, M.J., da Costa, L.N., & Huchra, J.P. 1995, *Astron. J.* **110**, 477
- [29] Bartlett, J.G., & Blanchard, A. 1996, *Astron. Astrophys.* **307**, 1
- [30] Peebles, P.J.E. 1994, *Ap.J.* **429**, 43
- [31] Branchini, E., & Carlberg, R.G. 1994, *Ap.J.* **434**, 37; Dunn, A.M., & Laflamme, R. 1995, *Ap.J. Lett.* **443**, 1
- [32] Shaya, E.J., Peebles, P.J.E., & Tully, R.B. 1995, *Ap.J.* **454**, 15
- [33] Primack, J.R. 1997, in *Formation of Structure in the Universe*, eds. A. Dekel and J.P. Ostriker (Cambridge University Press), in press
- [34] Dekel, A., Bertschinger, E., & Faber, S.M. 1990, *Ap.J.* **364**, 349; Dekel, A., Eldar, A., Kolatt, T., Willick, J.A., Faber, S.M., Courteau, S., & Burstein, D. 1977, in preparation
- [35] Dekel, A. 1994, *Annu. Rev. Astron. Astrophys.* **32**, 371; Dekel, A. 1996, in *Clustering in the Universe*, Moriond XX, eds. S. Morgatadeau and C. Balkowski (Editions Frontieres) p. 89; Dekel, A. 1997, in *Formation of Structure in the Universe*, eds. A. Dekel and J.P. Ostriker (Cambridge University Press), in press
- [36] Dekel, A., & Rees, M.J. 1993, *Ap.J. Lett.* **422**, L1
- [37] Bernardeau, F., Juszkiewicz, R., Dekel, A., & Bouchet, F.R. 1995, *MNRAS* **274**, 20
- [38] Nusser, A., & Dekel, A. 1993, *Ap.J.* **405**, 437
- [39] Willick, J.A., Courteau, S., Faber, S.M., Burstein, D., & Dekel, A. 1997, *Ap.J. Supp.*, in press
- [40] Willick, J.A. 1997, in *Formation of Structure in the Universe*, eds. A. Dekel and J.P. Ostriker (Cambridge University Press), in press

- [41] Kolatt, T., & Dekel, A. 1997, *Ap.J.* , in press (astro-ph/9512132); Zaroubi, S., Zehavi, I., Dekel, A., Hoffman, Y., & Kolatt, T. 1997, *Ap.J.* , in press (astro-ph/9610226)
- [42] Strauss, M.A., & Willick, J.A. 1995, *Phys. Rep.* **261**, 271
- [43] Strauss, M.A. 1997, in *Formation of Structure in the Universe*, eds. A. Dekel and J.P. Ostriker (Cambridge University Press), in press
- [44] Dekel, A., & Lahav O. 1997, in preparation
- [45] Dekel, A., Bertschinger, E., Yahil, A., Strauss, M.A., Davis, M., & Huchra, J. 1993, *Ap.J.* **412**, 1; Sigad, Y., Dekel, A., Strauss, M.A., & Yahil, A. 1997, in preparation
- [46] Willick, J.A., Strauss, M.A., Dekel, A., & Kolatt, T. 1997, in preparation
- [47] Davis, M., Nusser, A., & Davis, M. 1996, *Ap.J.* , in press (astro-ph/9604101)
- [48] Nusser, A., & Dekel, A. 1997, in preparation
- [49] White, S.D.M., Efstathiou, G., & Frenk, C.S. 1993, *MNRAS* **262**, 1023; Eke, V.R., Cole, S., & Frenk, C.S. 1996, astro-ph 9601088
- [50] Mo, H.J., Jing, Y.P., & White, S.D.M. 1996, *MNRAS* **282**, 1096
- [51] Lahav, O., Lilje, P.B., Primack, J.R., & Rees, M.J. 1991, *MNRAS* **251**, 128; Lightman, A.P., & Schechter, P.L. 1990, *Ap.J. Supp.* **74**, 831
- [52] Richstone, D., Loeb, A., & Turner, E.L. 1992, *Ap.J.* **393**, 477
- [53] Mohr, J.J., Evrard, A.E., Fabricant, D.G., & Geller, M.J. 1995, *Ap.J.* **447**, 8.
- [54] Jing, Y.P., Mo, H.J., Borner, G., & Fang, L.Z. 1995, *MNRAS* **276**, 417; Buote, D.A., & Xu, G. 1996, astro-ph/9609051
- [55] Katz, N., Quinn, T., Bertschinger, E., & Gelb, J.M. 1994, *MNRAS* **270**, L71; Eisenstein, D.J., & Loeb, A. 1995, *Ap.J.* **443**, 11
- [56] Steidel, C.C., Giavalisco, M., Pettini, M., Dickinson, M., & Adelberger, K.L. 1996, *Ap.J.* **462**, 17
- [57] Mo, H.J., & Fukugita, M 1996, *Ap.J. Lett.* **467**, 9
- [58] Lanzetta, K.M., Yahil, A., & Fernandez-Soto, A. 1996, *Nature* **381**, 759; Yahil, A. *et al.* 1996, in preparation
- [59] Zaroubi, S., Sugiyama, N., Silk, J., Hoffman, Y., & Dekel, A. 1997, *Ap.J.* , submitted (astro-ph/9610132)